Check for updates

Magnesium ferrichromate nanoparticles: an efficient and recyclable catalyst in the synthesis of pyrano[2,3-c] pyrazole derivatives

Ishita Yellapurkar[1] · Sonal Bhabal[1] · M. M. V. Ramana[1] · Kundan Jangam[2] ·
Vaibhav Salve[2] · Sunil Patange[3] · Paresh More[2]

Abstract

Magnetically separable magnesium ferrichromate nanoparticles ($MgFeCrO_4$ NPs) were synthesized by aqueous combustion synthesis (ACS) using glycine as the fuel. The as-synthesized powder was characterized using XRD, FTIR, SEM–EDX and SQUID techniques. Rietveld refinement studies inferred the single-phase cubic structure of the nanoferrite. Using Williamson–Hall plot, the lattice strain and the crystallite size were evaluated. Small value of lattice strain is indicative of absence of strain in the crystal lattice. The M–O bonding at the tetrahedral as well as the octahedral position was confirmed by FTIR Spectroscopy. Morphological investigations demonstrated sphere-like nanostructures with 50–100 nm particle size using SEM. Absence of any impurity in the EDX spectrum suggests formation of extremely pure $MgFeCrO_4$ NPs. The room temperature magnetization was studied using vibrating sample magnetometer, and the nanoferrite exhibits superparamagnetic behaviour. The pyrano[2,3-c]pyrazole derivatives were synthesized in water/ethanol solvent system using $MgFeCrO_4$ NPs heterogenous catalyst. A very short reaction time, maximum yield, easy method of separation of product and environmentally safer and milder reaction conditions are some of the advantages of our work along with the retention of catalytic activity up to five cycles.

✉ Paresh More
   paresh.m34@gmail.com

1   Department of Chemistry, University of Mumbai, Santacruz, Mumbai 400098, Maharashtra, India

2   Department of Chemistry, K. E. T's, Vinayak Ganesh Vaze College Autonomous , Mulund (E), Mumbai, Maharashtra, India

3   Department of Physics, Shrikrishna Mahavidyalaya Gunjoti, Gunjoti, Maharashtra, India

🍪 Springer

Graphic abstract

Synthesis of chromene derivatives using magnetically separable magnesium ferri-chromate (MgFeCrO$_4$).
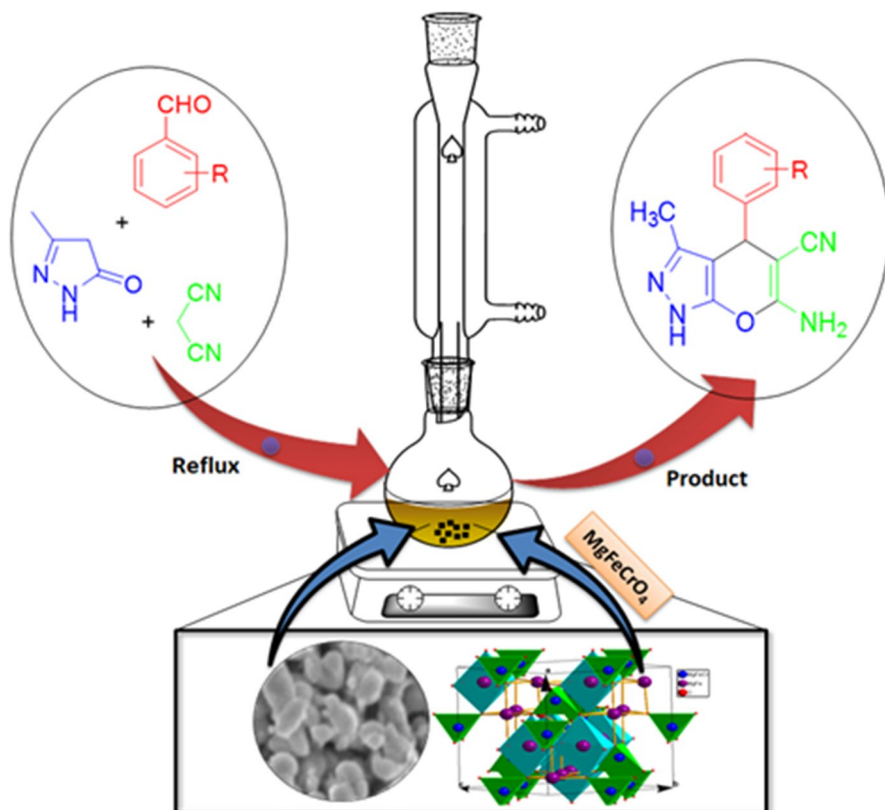
Keywords Ferrite · ACS Method · Pyrano[2,3-c]pyrazole Synthesis · Rietveld Refinement

Introduction

Heterocyclic compounds are extensively used as they find excellent applications in many pharmaceutical compounds. Primary reason for their versatile usage is owed to their ability to construct various structures which are necessary to accomplish certain significant functions [1, 2]. Heterocyclic molecules containing oxygen like pyrans and 4H-pyran-annulated heterocyclic scaffolds (4H-chromene moieties) piqued interest of researchers around the world, as they are omnipresent and provide appropriate biological activity. The structural features of these compounds are responsible for their cytotoxic [3], anti-tumour [4], anti-HIV [5], pharmacophore [6]

and analgesic activities [7]. Pyran-based heterocyclic compounds have been exhaustively used in the antimicrobial [8] pharmaceuticals [9] and drug industries [10]. In recent times, ''Multicomponent Reactions'' (MCRs) have surfaced as an alternative to the conventional methods for the preparation of diverse complex organic structures by the combination of three or more starting substrates [11]. The one-pot multicomponent reactions have intrigued many organic chemists due to their streamlined operation, simplified purification, reduced wastage, alleviated safety parameters and minimized duration [12, 13]. Any enolisable compound on reaction with a carbonyl compound and a compound containing an active methylene group in the presence of a base yields 2-amino-4H-chromene. Many researchers have developed procedures for the synthesis of pyrano[2,3-c]pyrazole derivatives via one-pot reaction involving Knoevenagel condensation of C–H activated compounds, aldehydes and malononitrile. Mehrabiand used sodium dodecyl sulphate (SDS) as the surfactant for synthesizing 3,4-dihydropyrano [c] chromene derivatives [14]. Tetrahydrobenzo [b] pyrans were synthesized by Gowravaram et al. using cerium (III) chloride as a catalyst [15]. Safaiee, et. al used novel dendrimer core of oxo-vanadium phthalocyanine magnetic nanoparticles in the synthesis of 3, 4 dihydropyrano [c] chromene derivatives [16]. Potassium phthalimide-N-oxyl was utilized as a catalyst for the synthesis of pyrano[2,3-c]pyrazole derivatives in water by Dekamin et al. [17]. 4H-pyrans and poly-substituted aniline derivatives were synthesized using silica nanoparticles as reusable catalyst by Banerjee et al. [18]. Most of the procedures exhibit attributes like very low yield of the desired product, long reaction times, tedious workup procedures, low recovery and very low reusability of the catalyst, thus generating a need for a coherent, multifaceted and eco-friendly process for the synthesis of 2-amino-4H-chromene derivatives. Magnetically separable spinel ferrite meets the above requirements, and few researchers have utilized it as an efficient catalyst [19–24].

Owing to the interaction between their magnetic properties and crystal chemistry, spinel ferrite nanoparticles are of considerable importance. On account of its grain size, occupancy of metal ions, and high chemical stability, spinel ferrite is considered a good candidate for synthesis of pyrano[2,3-c]pyrazole derivatives. Nevertheless, some of them also suffered from some apparent drawbacks, such as weak crystallinity, very restricted spectrum reaction range, low catalytic activity, etc. Therefore, an easy and schematic approach to assembling spinel ferrite nanostructures is highly desirable for effective catalysis in the chromene synthesis.

In continuation of our earlier research in synthesis of ferrites by ACS method and its application in environmental remediation [25], herein we report synthesis of $MgFeCrO_4$ NPs via ACS method. The synthesized nanoparticles were characterized using various techniques such as XRD, FTIR, SEM–EDX and VSM. As per the literature survey, this is the first study where catalytic efficiency of mixed metal oxide $MgFeCrO_4$NPs was investigated for the synthesis of pyrano[2,3-c]pyrazole derivatives with excellent yields ranging from 95 to 98%. Additionally, the process was characterized by shortened reaction times as compared to the results available in the literature to this day. The synthesis and characterization of the catalyst as well as its catalysis in the synthesis of pyrano[2,3-c]pyrazole derivatives are discussed in detail. The catalyst is easily isolated by magnetization. The recyclability of the

catalyst was checked for five cycles, and it showed excellent efficiency. The plausible mechanism of synthesis of pyrano[2,3-c]pyrazole derivatives over MgFeCrO$_4$ NPs is discussed in detail.

Experimental details

Materials and methods

All AR grade salts of Mg (NO$_3$)$_2$.6H$_2$O, Cr (NO$_3$)$_2$·9H$_2$O, Fe (NO$_3$)$_3$·9H$_2$O were procured from Merck (India). Chemicals required to synthesize pyrano[2,3-c]pyrazole derivatives were procured from Sigma Aldrich and were used without further purification. MgFeCrO$_4$NPs were synthesized using ACS method. AR grade salts of Mg (NO$_3$)$_2$.6H$_2$O, Cr (NO$_3$)$_2$·9H$_2$O, Fe (NO$_3$)$_3$·9H$_2$O were dissolved together (1:1:1 molar ratio) in distilled water to obtain a homogeneous solution. To this homogeneous solution, glycine was added and pH of the reaction mixture was adjusted to 7 with liq. NH$_3$ to form 'sol'. The sol was heated on the hot plate at 90˚C, to get a viscous gel which was then concentrated or matured to form the 'gel'. This homogeneous gel ignited on the hot plate, and after the complete combustion of glycine, MgFeCrO$_4$NPs were obtained [25]. The as-synthesized MgFeCrO$_4$NPs were then annealed in the furnace at 800 °C for five hours and later characterized by various analytical techniques.

Characterization of materials

The phase identification of the as-synthesized nanoparticles was achieved by Powder XRD. The XRD pattern was recorded on Philips (Xpert) X-ray diffractometer using Cu K-α radiation having wavelength 1.540 Å at room temperature. The analysis of magnetic properties was carried out by Quantum Design USA make SQUID system (Model MPMS XL). The morphology of nanoferrite was investigated by using JEOL JSM-7600F, FEG-SEM. FTIR spectra of the nanoparticles were recorded on 3000 Hyperion Microscope with vertex 80 FTIR using KBr pellets in the range of 400 to 4000 cm^{-1}. FTIR spectra of chromene were recorded on a Perkin Elmer (Model-Frontier) spectrometer. ^{1}H NMR (300 MHz) spectra were recorded on Bruker AVANCE spectrometer, whereas ^{13}C NMR (75 MHz) spectra were recorded on Bruker AVANCE spectrometer. Melting points of all the pyrano [2,3-c]pyrazole derivatives are uncorrected.

Catalytic activity of MgFeCrO$_4$NPs catalyst

Synthesis of pyrano[2,3-c]pyrazole derivatives

In a round-bottom flask, a mixture of pyrazolone **1** (5 mmol), aromatic aldehyde **2** (5 mmol), malononitrile **3** (5 mmol) and MgFeCrO$_4$ NPs (5 mol%) was placed in 1:1 water/ethanol mixture. The mixture was refluxed for appropriate period; after

the completion of the reaction (was monitored by TLC), the MgFeCrO$_4$ NPs were removed using an external magnet. The solvent was then evaporated, and the crude product was recrystallized from ethanol.
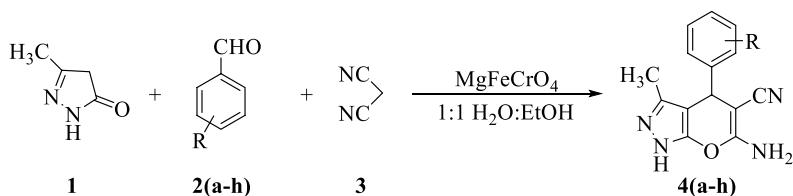
R =

a: 4-chlorophenyl   e: 3,4,5-trimethoxyphenyl
b: 4-methylphenyl   f: phenyl
c: 4-methoxyphenyl   g: 3-nitrophenyl
d: 3,4-dimethoxyphenyl   h: 2-methoxyphenyl

The spectroscopic data of the synthesized compounds are as follows:

6-amino-4-(4-chlorophenyl)-3-methyl-1,4-dihydropyrano[2,3-c]   pyrazole-5-carbonitrile (4a) *Molecular Formula* C$_{14}$H$_{11}$ClN$_4$O, *Colour* White. *IR (υmax, cm^{-1})* 3406(NH$_2$), 3306(NH), 2186(CN), 1599 (C=C). *^{1}H NMR (300 MHz, DMSO) δ* = 1.79 (s, 3H, CH$_3$), 4.63 (s, 1H, CH), 6.94 (s, 2H, NH$_2$), 7.19 (d, J = 8.4 Hz, 2H, Ar–H), 7.38 (d, J = 8.4 Hz, 2H, Ar–H), 12.15 (s, 1H, NH). *^{13}C NMR (75 MHz, DMSO) δ* = 9.69, 35.52, 56.74, 97.16, 120.61, 128.42, 129.32, 131.20, 135.66, 143.43,154.67,160.87.

6-amino-3-methyl-4-(p-tolyl)-1,4-dihydropyrano[2,3-c]pyrazole-5-carbonitrile (4b) *Molecular Formula* C$_{15}$H$_{14}$N$_4$O, *Colour* White. *IR (υmax, cm^{-1})* 3406(NH$_2$); 3313 (NH); 2191(CN), 1598 (C=C). *^{1}H NMR (300 MHz, DMSO) δ* = 1.78 (s, 3H, CH$_3$), 2.27 (s, 3H, CH$_3$), 4.54 (s, 1H, CH), 6.84 (s, 2H, NH$_2$),7.04 (d, J = 8.4 Hz, 2H, Ar–H), 7.11 (d, J = 8.4 Hz, 2H, Ar–H), 12.08 (s, 1H, NH). *^{13}C NMR (75 MHz, DMSO) δ* = 9.72, 20.59, 35.81, 57.34, 97.68, 120.77, 127.32, 128.95, 135.50, 135.67, 141.45, 154.72, 160.73.

6-amino-4-(4-methoxyphenyl)-3-methyl-1,4-dihydropyrano[2,3-   c]pyrazole-5-carbonitrile (4c) *Molecular Formula* C$_{15}$H$_{14}$N$_4$O$_2$, *Colour* White. *IR (υmax, cm^{-1})* 3482(NH$_2$); 3250 (NH); 2189(CN), 1596 (C=C). *^{1}H NMR (300 MHz, DMSO) δ* = 1.78 (s, 3H, CH$_3$), 3.72 (s, 3H, CH$_3$), 4.53 (s, 1H, CH), 6.83 (s, 2H, NH$_2$), 6.86 (d, J = 8.6 Hz,2H, Ar–H), 7.07 (d, J = 8.6 Hz, 2H, Ar–H), 12.09 (s, 1H, NH). *^{13}C NMR (75 MHz, DMSO) δ* = 9.69, 35.38, 54.95, 57.57, 97.84, 113.72, 120.80, 128.45, 135.55, 136.42, 154.70, 157.92, 160.64.

6-amino-4-(3,4-dimethoxyphenyl)-3-methyl-1,4-dihydropyrano[2,3-   c]pyrazole-carbonitrile (4d) *Chemical Formula* C$_{16}$H$_{16}$N$_4$O$_3$, *Colour* White. *IR (υmax, cm^{-1})* 3372(NH$_2$); 3135 (NH); 2184(CN), 1596 (C=C). *^{1}H NMR (300 MHz, DMSO) δ* = 1.82 (s, 3H, CH$_3$), 3.69 (s, 3H, CH$_3$), 3.72 (s, 3H, CH$_3$), 4.55 (s, 1H,

CH), 6.68 (dd, J = 8.2, 2.6 Hz, 1H, Ar–H), 6.75 (d, J = 8.2 Hz, 1H, Ar–H), 6.83 (s, 2H, NH$_2$), 6.89 (d, J = 2.6 Hz, 1H, Ar–H), 12.08 (s, 1H, NH). ^{13}C NMR (75 MHz, DMSO) δ = 9.80, 35.79, 55.40, 55.43, 57.38, 97.67, 111.16, 111.70, 119.44, 120.82, 135.59, 136.86, 147.52, 148.50, 154.69, 160.71.

6-amino-3-methyl-4-(3,4,5-trimethoxyphenyl)-1,4-dihydropyrano[2,3-c]pyrazole-carbonitrile (4e) *Chemical Formula* C$_{17}$H$_{18}$N$_4$O$_4$, *Colour* White. *IR (υmax, cm^{-1})* 3477(NH$_2$); 3305 (NH); 2187(CN), 1596 (C=C). ^1H NMR (300 MHz, DMSO) δ = 1.87 (s, 3H, CH$_3$), 3.64 (s, 3H, CH$_3$), 3.72 (s, 6H, CH$_3$), 4.58 (s, 1H, CH), 6.47 (s, 2H, Ar–H), 6.86 (s, 2H, NH$_2$), 12.09 (s, 1H, NH). ^{13}C NMR (75 MHz, DMSO) δ = 9.89, 36.44, 55.80, 56.91, 59.92, 97.29, 104.59, 120.80, 135.70, 136.16, 140.03, 152.76, 154.68, 160.94.

6-amino-3-methyl-4-phenyl-1,4-dihydropyrano[2,3-c]pyrazole-5-carbonitrile (4f) *Chemical Formula* C$_{14}$H$_{12}$N$_4$O, *Colour* White. *IR (υmax, cm^{-1})* 3369(NH$_2$); 3164(NH); 2191(CN), 1595 (C=C). ^1H NMR (300 MHz, DMSO) δ = 1.78 (s, 3H, CH$_3$), 4.59 (s, 1H, CH), 6.88 (s, 2H, NH$_2$), 7.22 (m, 5H, Ar–H), 12.10 (s, 1H, NH). ^{13}C NMR (75 MHz, DMSO) δ = 9.70, 36.20, 57.15, 97.60, 120.75, 126.69, 127.43, 128.40, 135.53, 144.41, 154.73, 160.83,

6-amino-3-methyl-4-(3-nitrophenyl)-1,4-dihydropyrano[2,3-c]pyrazole-5-carbonitrile (4 g) *Molecular Formula* C$_{14}$H$_{11}$N$_5$O$_3$, *Colour* Yellow. *IR (υmax, cm^{-1})* 3472(NH$_2$); 3287 (NH); 2193(CN), 1594 (C=C). ^1H NMR (300 MHz, DMSO) δ = 1.81 (s, 3H, CH$_3$), 4.88 (s, 1H, CH), 7.06 (s, 2H, NH$_2$), 7.63 (m, J = 8.36, 8.0 Hz,1H, Ar–H), 7.68 (m, J = 8.0,1.53,1.38 Hz, 1H, Ar–H), 8.10 (m, J = 1.70,1.53 Hz, 1H, Ar–H), 8.13 (m, J = 8.36,1.70,1.38 Hz, 1H, Ar–H), 12.21 (s, 1H, NH). $^{13}CNMR$ (75 MHz, DMSO) δ = 9.71, 35.61, 56.11, 96.63, 120.47, 121.81, 121.95, 130.21, 134.35, 135.86, 146.79, 147.85, 154.66, 161.11.

6-amino-4-(2-methoxyphenyl)-3-methyl-1,4-dihydropyrano[2,3-c]pyrazole-5-carbonitrile (4 h) *Chemical Formula* C$_{15}$H$_{14}$N$_4$O$_2$, *Colour* White. *IR (υmax, cm^{-1})* 3425 (NH$_2$); 3306 (NH); 2186(CN), 1596 (C=C). ^1H NMR (300 MHz, DMSO) δ = 1.80 (s, 3H, CH$_3$), 3.80 (s, 3H, CH$_3$), 4.98 (s, 1H, CH), 6.67 (s, 2H, NH$_2$), 6.88 (m, J = 7.98, 7.4, 1.28 Hz, 1H, Ar–H), 6.97 (m, J = 8.2,1.28 Hz, 1H, Ar–H), 7.15 (m, J = 7.98, 1.28 Hz, 1H, Ar–H), 7.20 (m, J = 8.2, 7.4, 1.28 Hz, 1H, Ar–H), 11.95 (s, 1H, NH). ^{13}C NMR (75 MHz, DMSO) δ = 9.46, 55.42, 56.54, 95.51, 97.70, 111.00, 120.67, 120.72, 127.72, 128.53, 132.03, 134.93, 155.02, 156.24, 161.37.
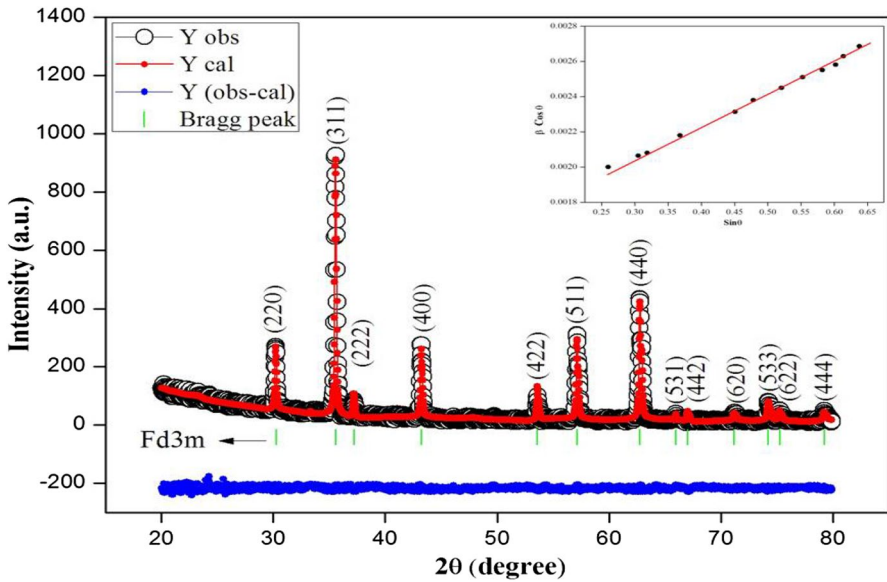
Fig. 1 Rietveld refinement of XRD pattern and inset Williamson–Hall plot of $MgFeCrO_4$ nanoferrite

Result and discussion

Characterization of $MgFeCrO_4$ catalyst

The phase identification of $MgFeCrO_4$ NPs has been investigated using XRD. Figure 1 displays structurally refined X-ray diffraction patterns of $MgFeCrO_4$ NPs. It is clear from the figure that the sample is without any secondary planes and displays the reflection from the planes (220), (311), (222), (400), (422), (511), (440), (531), (533) and (444) which corresponds to face-centred cubic. Thus, $MgFeCrO_4$ is a single-phase cubic spinel structure with Fd3m space group as shown in Fig. 1. On carefully observing XRD the peaks widen at the bottom, which is a proof of the existence of nanoscale dimensioned particles. The reliability of refinement was characterized by the consideration of the various R-factors such as expected factor (R_{exp}), profile factor (R_{wp}) and goodness-of-fit (χ^2). The value of goodness factor (χ^2) is equal to 1.03, which is attributed as an excellent value for the estimations. Lower the value of χ^2 better is the profile fitting; hence, the procedure adopted for profile fitting is by minimizing the χ^2 function. The theoretical lattice constant (a_{th}) and the experimental lattice constant (a_{exp}) are depicted in Table 1, and the values are in very close agreement with each other. Further, a_{th} is greater than a_{exp}; this is because the perfect spinel structure was assumed for calculation of a_{th} with cations and anions as a rigid sphere [26]. The results obtained on the X-ray diffraction of $MgFeCrO_4$ nanoferrite systems in the Rietveld refinement are listed in Table 1. Williamson–Hall plot of the catalyst ($MgFeCrO_4$) is in the Inset of Fig. 1. The values of average crystallite size and

Table 1 The crystal data and refinement factors MgFeCrO$_4$ obtained from X-ray powder diffraction data

Parameter	Result	Description of parameters
Crystal system	Single-phase cubic	–
Space group	$Fd3m$	–
a (Å)	8.3674	Edge length along X–direction
b (Å)	8.3674	Edge length along Y–direction
c (Å) ath	8.3674 8.3886	Edge length along Z–direction theoretical lattice constant
α (degree)	90.0	Interfacial angle
β (degree)	90.0	Interfacial angle
γ (degree)	90.0	Interfacial angle
V (Å^3)	584.69	Volume of unit cell
R_P	10.6	R_p (profile factor) $= 100[\Sigma|y_i\text{-}y_{ic}|/\Sigma|y_i|]$, where y_i is the observed intensity and y_{ic} is the calculated intensity at the ith step
R_{wp}	15.6	R_{wp} (weighted profile factor) $= 100[\Sigma\omega_i|y_i\text{-}y_{ic}|2/\Sigma\omega_i(y_i)^2]^{1/2}$, where and is variance of the observation
R_{exp}	15.1	R_{exp} (expected weighted profile factor) $= 100[(n\text{-}p)/\Sigma\omega_i(y_i)^2]^{1/2}$, where '$n$' and '$p$' are number of profile points and refined parameters, respectively
χ^2	1.03	$\chi^2 = \Sigma\omega_i(y_i\text{-}y_{ic})^2$
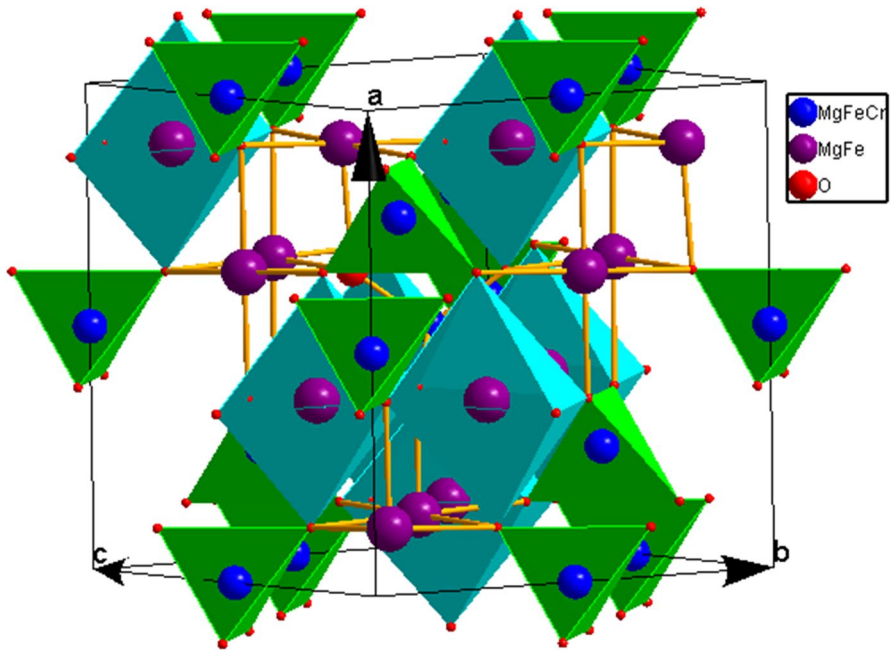
Fig. 2 Three-dimensional crystal structure of Cubic spinel belonging to Fd3m space group of $MgFeCrO_4$. Interstitial positions partially occupied by tetrahedral-A and octahedral-B atom

r.m.s. strain are 70 nm and 0.00029033, respectively, obtained from a linear least square fitting to $\eta \cos\theta - \sin\theta$. The r.m.s. strain value is extremely low indicating very stable structure of $MgFeCrO_4$, which may be due to the method of preparation of synthesis (ACS method).

Table 2 The crystal data and refinement factors $MgFeCrO_4$ obtained from X-ray powder diffraction data

Sr. No	Parameter	Results
1	Site occupancy tetrahedral (A)	$Mg_{0.5}Fe_{0.5}$
2	Site occupancy octahedral (B)	$Mg_{0.5}Cr_{1.0}Fe_{0.5}$
3	Tetrahedral radius (r_A)	0.6950
4	Octahedral radius (r_B)	0.6625
5	Crystalline size from Scherrer's equation	16.19
6	Crystalline size form Williamson-Hall plot	70 nm
7	r.m.s. Strain	2.9033×10^{-4}
8	Oxygen positional parameter (U)	0.3437
9	Tolerance factor (T)	1.0512
10	X- ray density	4.455
11	Saturation magnetization (Ms)	0.96 emu/g
12	Remnant magnetization (Mr)	0.094 emu/g
13	Squareness ratio (Mr/Ms)	0.098
14	Coercivity (Hc)	52.25 Oe

The crystal structure of MgFeCrO$_4$ NPs obtained by Rietveld refinement is shown in Fig. 2. The crystallite size (using Scherrer's equation and Williamson Hall plot), the X-ray density (dx), the cation distribution, tetrahedral radius (r_A), octahedral radius (r_B), oxygen positional parameter (u), the tolerance factor (T), saturation magnetization (Ms), coercivity (Hc), squareness ratio (Mr/Ms), Remnant magnetization (Mr) were calculated from the expression discussed elsewhere [26] and are depicted in Table 2.

The site occupancy of MgFeCrO$_4$ system was calculated using the Bertaut method [27]. Excellent knowledge on distribution of cations can be obtained by matching the intensity ratio (experimental and calculated) for reflections whose intensities (i) vary with the distribution of cations in the opposite ways, (ii) are almost independent of the oxygen position parameter and (iii) do not remarkably differ. In MgFeCrO$_4$ NPs, equal concentrations of Mg^{2+} and Fe^{3+} transfer to tetrahedral and octahedral site, whereas the entire Cr^{3+} ions retain at the octahedral site. Retaining of Cr^{3+} ions at octahedral site in ferrichromates was reported by various researchers [28–30]. The radius of the oxygen ion ($R_0 = 1.32$), tetrahedral radius (r_A), the lattice constant (a) and the oxygen positional parameter 'u' can be calculated from the expression discussed elsewhere [26]. The calculated oxygen positional parameter is 0.3891. In most of the spinel oxides, the size of oxygen ion is found to be larger than the other metallic ions. The value of oxygen positional parameter is approximately equal to 0.375 Å in spinel structures. To have this value, the arrangement O^{2-} ions should be ideal, the packing should be exactly cubic; however, in observed spinel lattice this pattern slightly deviate from ideal pattern and gets slightly deformed. Our value of oxygen positional parameters (u) is greater than ideal value; this may be due to various reasons, experimental error or measurement errors. In most samples, u > 0.375 is obtained due to a very little displacement of anions because of tetrahedral interstitials expansion. In MgFeCrO$_4$, the positional coordinates of oxygen (u) is greater than 0.375 which can be ascribed to the displacement of anions from the ideal positions [26]. The lattice constants (a) and the oxygen positional parameter (u) values reflect that there is no disturbance in the lattice, which is further confirmed from Tolerance factor.

Tolerance factor (T) for the ferrite nanoparticles was determined using following equation.

$$T = \frac{1}{\sqrt{3}}\left(\frac{r_A + R_0}{r_B + R_0}\right) + \frac{1}{\sqrt{2}}\left(\frac{R_0}{r_A + R_0}\right)$$

In the equation, r_A is radius of tetrahedral site, r_B radius of octahedral site, and the radius of oxygen ion is R_0. It is clear from the literature survey that the spinel is defect free if tolerance factor is nearly equal to one. The catalyst MgFeCrO$_4$ is defect free as the tolerance factor is almost unity (Table 2).

Morphological study of the as-synthesized MgFeCrO$_4$NPs was performed using the scanning electron microscope (SEM). Figure 3 displays the SEM image and the corresponding EDX spectra of MgFeCrO$_4$. The SEM image in Fig. 3a indicates irregular shaped nanostructures have been formed. Furthermore, it has been found that the nanoparticles are aggregated, and the maximum particles are spherical
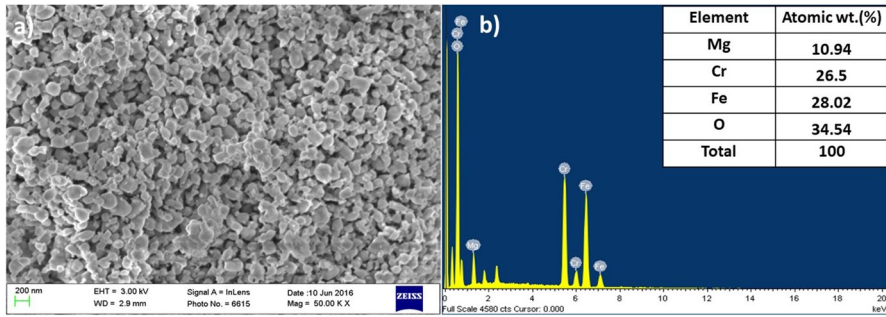
Fig. 3 **a** FESEM **b** EDX- image of as-synthesized MgFeCrO$_4$ nanoferrite

in shape. The average size of irregularly formed nanoparticles ranges from 50 to 80 nm. The corresponding EDX spectra of MgFeCrO$_4$ are shown in Fig. 3b. The EDX spectra of nanomaterials give an indication of the elementary composition. It can be seen from the figure that the elementary composition of Mg, Cr, Fe and O was found to be 10.94, 26.50, 28.02 and 34.54, respectively. The stoichiometric ratio observed in the EDX spectra is closely correlated with the theoretical content. Absence of impurity peak in the EDX spectra supports the formation of very pure MgFeCrO$_4$ NPs.

The structure of as-synthesized compounds can be analysed using FTIR spectroscopy. FTIR spectra of MgFeCrO$_4$NPs was recorded in 4000–400 cm^{-1} range (Fig. 4a). The higher frequency band at 593.6 cm^{-1} is assigned to (M$_{tet}$-O) bond vibration, whereas the band at lower frequency band at 436.8 cm^{-1} corresponds to (M$_{oct}$–O) bond vibration as depicted in Fig. 4b, where the range is from 1000–400 cm^{-1}. The weak bands were observed at 3400 cm^{-1}, 1600 cm^{-1} and 1380 cm^{-1} correspond to the hydroxyl, carboxyl and nitrate ions, respectively [31].
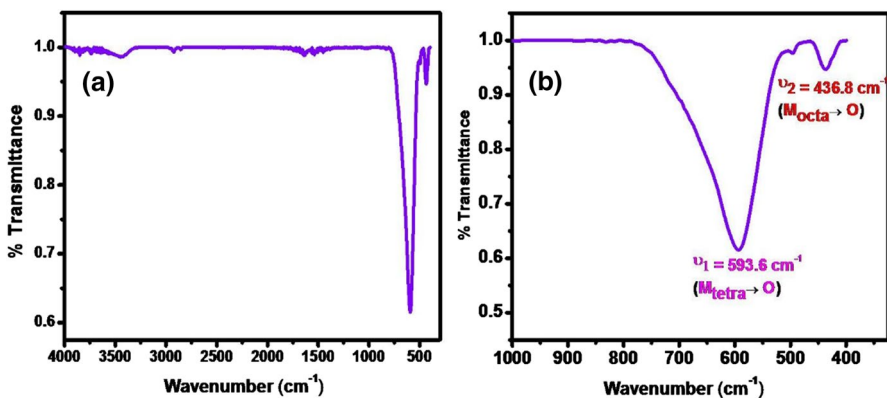
Fig. 4 FTIR absorption spectra of MgFeCrO4 nanoferrite **a** in the range of 4000–400 cm^{-1} and **b** in the range of 1000–400 cm^{-1}

All carboxyl, hydroxyl and nitrate groups occurred at a very low intensity due to the extremely high temperature produced during combustion [32]. In addition, the lower band at 1590 cm^{-1} is allocated for H–O–H bending vibrations due to humidity absorption [33]. The HOH bond-bending mode of adsorbed water molecules was found in the range from 1500 to 1700 cm^{-1} [34].

Room temperature magnetic hysteresis loop and expanded view of hysteresis loop of MgFeCrO$_4$NPs are depicted in Fig. 5a and Fig. 5b, respectively. Very low value of saturation magnetization (Ms) is due to the weakening of exchange interaction due to non-magnetic Cr^{3+} ions. Cation distribution of the MgFeCrO$_4$ system is responsible for a very high coercivity (Hc). Similar observation in coercivity were reported by Banerjee and O'Reilly [35]. The anisotropy constant K is very low, whereas the squareness ratio (Mr/Ms) ratio was found to be very close to 0.10. This low value suggests that the ferrite nanoparticles are superparamagnetic [36, 37]. It is well-established fact that in the case of interacting superparamagnetic particles, Mr/Ms ratio and the K values gets reduced because of demagnetizing effect [38]. The effect of which is the ratio of Mr/Ms is nearly equal to 0.10, when magnetic field is removed such samples loses it magnetization. Furthermore, in the presence of external field these samples react very quickly and allow very easy magnetization and demagnetization with almost zero hysteresis loss, which makes superparamagnetic ferrites a perfect material in the application of nanoelectronics and spintronics.
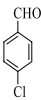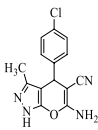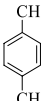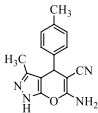
Catalysis
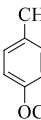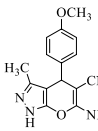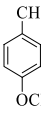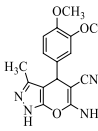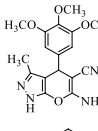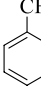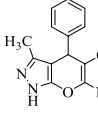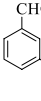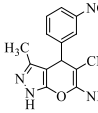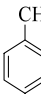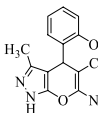
As-synthesized MgFeCrO$_4$NPs were employed as a catalyst in the three-component one-pot synthesis of pyrano[2,3-c] pyrazole derivatives (Table 3) [39–46].

The reaction of pyrazolone, p-chlorobenzaldehyde and malononitrile was taken as a module. Foremost, the effect of amount of catalyst was examined. There was no reaction in the absence of the catalyst (Table 4, entry 1). 2.5 mol % catalyst gave 74% yield (Table 4, entry 2). The highest yield (85%) was obtained when 5 mol%
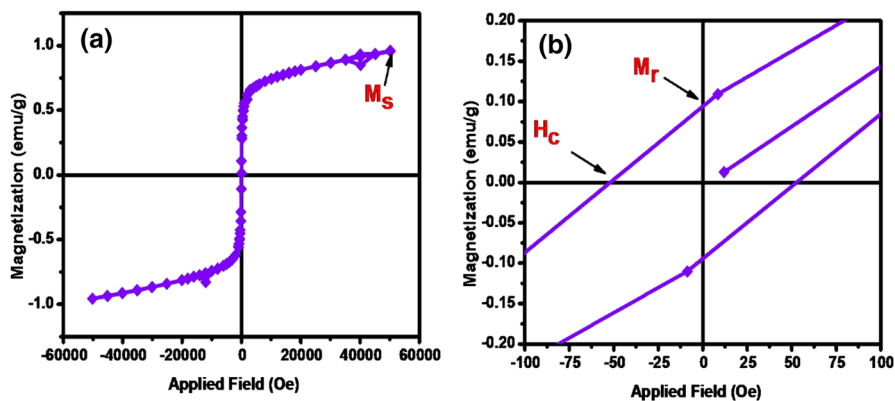
Fig. 5 **a** Hysteresis loop of as prepared MgFeCrO$_4$. **b** Expanded view of Hysteresis loop recorded at room temperature

Table 3 Synthesis of pyrano[2,3-c]pyrazole from various aromatic aldehydes malononitrile and pyrazolone

Entry	Aromatic aldehyde	Product	Time (min)	Melting point (°C)	Yield (%)	References
1			5	233–235	98	[39]
2			5	206–208	95	[40]
3			5	208–210	96	[41]
4			5	190–192	94	[42]
5			5	209–210	95	[43]
6			8	243–245	90	[44]
7			5	233–235	93	[45]
8			5	251–252	96	[46]

catalyst was used (Table 4, entry 3). However, on increasing the amount of catalyst to 10 mol % no significant increase in the yield was observed (Table 4, entry 4). Thus, 5 mol % was the optimum amount of catalyst which was then employed in further studies. The effect of different reaction times was also studied. The reaction yielded 82% product in 3 min (Table 4, entry 5). The maximum yield of the product was obtained in 5 min (Table 4, entry 6). However, prolonged reaction time (10 min) showed no significant increase in the yield (Table 4, entry 7). The effect of various solvents on the reaction was also investigated. Poor yields were observed

Table 4 Optimization of the catalyst for the synthesis of chromenes[a]

Entry	Catalyst (mol%)	Solvent	Temp (°C)	Time (min)	Yield (%)[b]
	Effect of amount of catalyst				
1	0	Ethanol	Reflux	No reaction	–
2	2.5	Ethanol	Reflux	5	74
3	5	Ethanol	Reflux	5	85
4	10	Ethanol	Reflux	5	87
	Effect of time				
5	5	Ethanol	Reflux	3	82
6	5	Ethanol	Reflux	5	89
7	5	Ethanol	Reflux	10	90
	Effect of solvent				
8	5	Water	Reflux	5	47
9	5	DCM	Reflux	5	75
10	5	Methanol	Reflux	5	85
11	5	Acetonitrile	Reflux	5	80
12	5	Toluene	Reflux	5	60
	Effect of solvent mixture (1:1)				
13	5	Water/ethanol	Reflux	5	98
14	5	Water/methanol	Reflux	5	88
15	5	Water/acetonitrile	Reflux	5	75
	Effect of water/ethanol ratio				
16	5	1:9	Reflux	5	83
17	5	2:8	Reflux	5	81
18	5	3:7	Reflux	5	82
19	5	4:6	Reflux	5	80
20	5	6:4	Reflux	5	56
21	5	7:3	Reflux	5	55
22	5	8:2	Reflux	5	50
23	5	9:1	Reflux	5	48
	Effect of temperature				
24	5	1:1 Water/ethanol	RT	No reaction	–
25	5	1:1 Water/ethanol	40	5	30
26	5	1:1 Water/ethanol	60	5	50

[a]Reaction Conditions: pyrazolone (1 mmol), p-chlorobenzaldehyde (1 mmol), malononitrile (1 mmol) and catalyst $MgFeCrO_4$ under reflux

[b]Isolated yield

in water and toluene (Table 4, entries 8 and 12). Moderate yields were obtained in DCM (Table 4, entry 9). Methanol and acetonitrile gave better results with 85% and 80% yields respectively (Table 4, entries 10 and 12). Since polar solvent media are known to obtain maximum catalytic activity for cyclization reactions [47], the effect of solvent mixtures of water with other solvents in the ratio of 1:1 was also studied. It can be clearly seen that water and ethanol solvent mixture gave the best yield of

98% (Table 4, entry 13), whereas methanol and acetonitrile both gave poorer yields (Table 3, entries 10 and 11). The effect of water–ethanol solvent mixture for optimization of water/ethanol ratio was further investigated. In solvent mixtures containing higher amount of ethanol, better yields were obtained (Table 4, entries 16 to 19) as compared to mixtures containing higher amount of water which showed poorer yields (Table 4, entries 21–23). However, highest yield of 98% was the one obtained for 1:1 water/ethanol solvent mixture (Table 4, entry 13). Finally, the effect of temperature on the reaction was examined. At room temperature, the reaction does not proceed at all (Table 4, entry 24), and 30% and 50% yields were observed at temperatures 40 °C and 60 °C, respectively (Table 4, entries 25 and 26). The highest yield of the reaction, however, was 98% which was obtained under reflux conditions (Table 4, entry 13). The reaction condition was optimized (reflux time: 5 min; catalyst quantity: 5 mol%; system: equivalent quantity of water and ethanol), and the catalyst was employed in the synthesis of different chromene derivatives (Table 3). The electron donating substituents resulted in slightly higher yields (Table 3, entries 1–5, 8) as compared to electron-withdrawing substituents (Table 3, entries 6 and 7).

Comparative studies

Table 5 summarizes the comparative studies of pyrano[2,3-c]pyrazole derivatives synthesis using different catalysts, already reported in literature [48–59]. The main advantage of the present protocol is the separation of the catalyst from the reaction medium as compared to the conventional separation techniques of filtration, centrifugation and solvent extraction which are tiresome and time-consuming (Table 5, entries 5, 7 and 9 to 14). The catalyst was separated using an external magnet. The product obtained is purified by recrystallization method, thus avoiding tedious chromatographic purification techniques. The reaction time is significantly less (Table 5, entries 1, 4 to 8 and 10 to 14), and the yields obtained are much better (Table 5, entries 2, 3, 5, 7 to 9, 11, 12 and 14). To sum up, operational simplicity, very high yields, very small reaction times, absence of traditional separation and purification methods and ease of workup are the advantages of our method.

Reusability studies of the catalyst

Figure 6 shows the reusability of the catalyst up to 5 cycles. The reaction studied was p-chlorobenzaldehyde, pyrazolone and malononitrile refluxed under optimal conditions. After each cycle, the catalyst was separated magnetically, washed thoroughly with distilled water and finally by ethanol. The catalyst was then dried in an oven at 120 °C for two hours. The recovered catalyst was then reused for further reactions under the same reaction conditions, and consistent catalytic activity was observed up to five cycles. The catalyst showed 98%, 96%, 95%,92% and 88% yield for 1st, 2nd, 3rd, 4h, and 5th cycle, respectively. After the fifth cycle, the catalytic efficiency was observed to decrease.

Table 5 Comparison of reported methods of the synthesis of pyrano[2,3-c]pyrazole derivatives with the present protocol

| Sr. No	Catalyst	Reaction conditions	Catalyst separation	Time (min)	Yield (%)	References
1	$CuFe_2O_4$	Water	Magnetic separation	120	95	[48]
2	$Ni_{0.5}Zn_{0.5}Fe_2O_4$ @ Hap-Cs_2CO_3	1:1 Water/EtOH, RT	Magnetic separation	10	92	[49]
3	$Ni_{0.5}Zn_{0.5}Fe_2O_4$ @ SiO_2–PPA	Water, RT	Magnetic separation	12	91	[50]
4	γ-alumina	Water, reflux	Filtration	35	90	[51]
5	Imidazole	Water, 80 °C	Filtration	20	90	[52]
6	Molecular sieves MS 4A	EtOH, reflux	Solvent extraction	60	90	[53]
7	β-cyclodextrin	9:1 Water:EtOH, 80 °C	Filtration	15	92	[54]
8	Amberlyst A21 (Ion exchange resin)	EtOH, RT	Filtration	20	98	[55]
9	L-Proline	Water	Filtration	10	90	[56]
10	Bovine serum albumin	7:3 Water/EtOH, 40 °C	Filtration	60	94	[57]
11	Lipase	EtOH, 30 °C	Centrifugation	60	95	[58]
12	DES (1:2 choline chloride/urea)	80 °C	Solvent extraction	20	91	[59]
13	5 mol% $MgFeCrO_4$	1:1 H_2O:EtOH, reflux	Magnetic separation	5	98	Present work
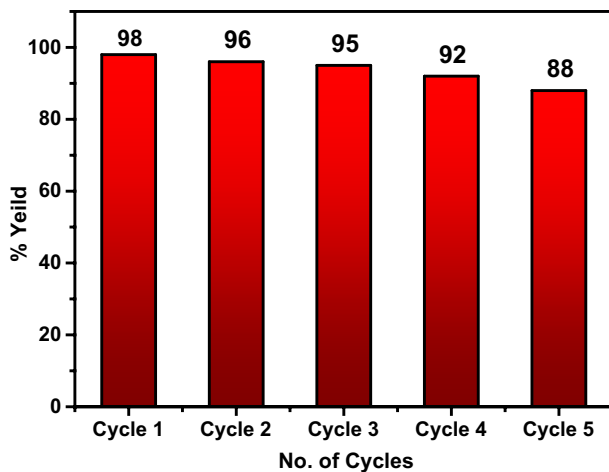
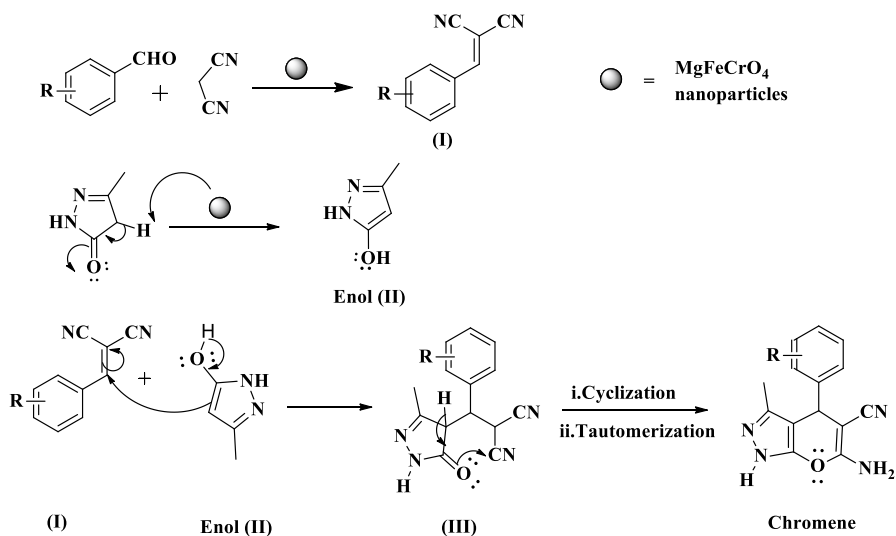**Fig. 6** Reusability of MgFeCrO4 nanoferrite for five cycles

Fig. 7 Plausible mechanism for synthesis of pyrano[2,3-c]pyrazole derivatives

Plausible mechanism for synthesis of pyrano[2,3-c] pyrazole derivatives

The synthesis of pyrano[2,3-c]pyrazole derivatives is a traditionally base catalysed reaction which does not proceed in the absence of a base. The plausible mechanism of synthesis of pyrano[2,3-c]pyrazole derivatives using $MgFeCrO_4NPs$ is shown in Fig. 7. The catalyst $MgFeCrO_4NPs$ acts as a base to abstract the most acidic proton from malononitrile and subsequently form the Knoevenagel product (**I**). In the second step of mechanism, base catalyst abstract the proton from alpha position to

form enol (**II**). The reaction is a tandem reaction which further involves the Michael addition of pyrazolone to the Knoevenagel product (**I**) to form product **III** followed by the intramolecular nucleophilic attack of carbonyl oxygen on –C≡N. The product **III** then undergoes Thorpe – Ziegler cyclization and tautomerization to yield pyrano[2,3-c]pyrazole.

Conclusion

Magnetically separable $MgFeCrO_4$NPs were synthesized using ACS method. The $MgFeCrO_4$NPs was successfully employed as a catalyst in the present synthetic protocol. The distinguishing feature of the catalyst is ease of separation from the reaction mixture. The ease of operation and very high yields make the catalyst superior over other catalyst. Also, the key features of the present protocol are shorter reaction times, wider substrate scope, cleaner reaction without the need of any traditional separation and purification methods which adhere to the green chemistry principles.

Data availability statement The data that support the findings of this study are available on request from the corresponding author. The data are not publicly available due to privacy or ethical restrictions.

Declarations

Conflict of interest The authors declare that they have no conflict of interest.

References

1. F. Al-Assar, K.N. Zelenin, E.E. Lesiovskaya, I.P. Bezhan, B.A. Chakchir, Pharm. Chem. J. **36**, 598 (2002)
2. R.P. Jain, J.C. Vederas, Bio-org. Med. Chem. Lett. **14**, 3655 (2004)
3. T. Raj, R.K. Bhatia, A. Kapur, M. Sharma, A.K. Saxena, M.P. Ishar, Eur. J. Med. Chem. **2**(45), 790 (2010)
4. S.J. Mohr, M.A. Chirigos, F.S. Fuhrman, J.W. Pryor, Cancer Res. **35**, 3750 (1975)
5. M.T. Flavin, J.D. Rizzo, A. Khilevich, A. Kucherenko, A.K. Sheinkman, V. Vilaychack, L. Lin, W. Chen, E.M. Greenwood, T. Pengsuparp, J.M. Pezzuto, S.H. Hughes, T.M. Flavin, M. Cibulski, W.A. Boulanger, R.L. Shone, Xu ZQ. J. Med. Chem. **39**, 1303 (1996)
6. A.G. Martinez, L. Marco, J. Bio org. Med. Chem. Lett. **7**, 3165 (1997)
7. L. Bonsignore, G. Loy, D. Secci, A. Calignano, Eur. J. Med. Chem. **28**, 517 (1993)
8. I.H. ElAzab, M. Youssef, M. Amin, Molecules **19**, 19648 (2014)
9. A. Shaabani, R. Ghadari, A. Sarvary, A.H. Rezayan, J. Org. Chem. **74**, 4372 (2009)
10. M. Costa, T. Dias, A. Brito, F. Proenca, Eur. J. Med. Chem **123**, 487 (2016)
11. M. Syamala, Org. Prep. Proceed. Int. **41**(1), 1 (2009)
12. R.W. Armstrong, A.P. Combs, P.A. Tempest, S.D. Brown, T.A. Keating, Acc. Chem. Res. **29**, 123 (1996)
13. S. Kamijo, Y. Yamamoto, J. Am. Chem. Soc. **124**, 11940 (2002)
14. H. Mehrabi, H. Abusaidi, J. Iran. Chem. Soc. **7**(4), 890 (2010)
15. S. Gowravaram, K. Arundhathi, K.B.S. Sudhakar, J.S. Yadav, Synth. Commun. **39**, 433 (2009)

16. M. Safaiee, M.A. Zolfigol, F. Afsharnadery, S. Baghery, RSC Adv. **5**, 102340 (2015)
17. M.G. Dekamin, M. Eslami, A. Maleki, Tetrahedron **69**, 1074 (2013)
18. S. Banerjee, A. Horn, H. Khatri, G.A. Sereda, Tetrahedron Lett. **52**, 1878 (2011)
19. R. Fareghi-Alamdari, N. Zekri, F. Mansouri, Res Chem Intermed. **43**, 6537 (2017)
20. H. Ahankar, A. Ramazani, K. Slepokura, T. Lis, J. Chem. **42**, 719 (2018)
21. Y. Pourshojaei, F. Zolalal, K. Eskandari, M. Talebi, L. Morsali, M. Amiri, A. Khodadadi, R. Sham-simeymandi, E. Faghih-Mirzaei, A. Asadipour, J. Nanosci. **20**, 3206 (2020)
22. J. Rajput, P. Arora, G. Kaur, M. Kaur, Ultrason Sonochem **26**, 229 (2015)
23. Z. Zarnegar, J. Safari, J. Mol. Struc. **1072**, 53 (2014)
24. S. Rostamizadeh, N. Zekri, Res. Chem. Intermed. **42**, 2329 (2016)
25. K. Jangam, K. Patil, S. Balgude, S. Patange, P. More, J. Phys. Chem. Solids. **148**, 109700 (2021)
26. K. Jangam, K. Patil, S. Balgude, S. Patange, P. More, RSC Adv. **10**, 42766 (2020)
27. L. Weil, F. Bertaut, L. Bochirol, J. Phys. Radium. **11**, 208 (1950)
28. S.H. Lee, S.J. Yoon, G.J. Lee, H.S. Kim, C.H. Yo, K. Ahn, D.H. Lee, K.H. Kim, Mat. Chem. Phys. **61**, 147 (1999)
29. M.K. Fayek, S.S. Ata Allah, Phys. Stat. Sol. 198, 457 (2003).
30. A. Gismelseed, A. Yousif, Phys. B **370**, 215 (2005)
31. R. Waldron, Phys. Rev. **99**, 1727 (1955)
32. B. Pourgolmohammad, S.M. Masoudpanah, M.R. Aboutalebi, Ceram. Int. **43**(4), 3797 (2017)
33. T. Slatineanu, A.R. Iordan, M.N. Palamaru, O.F. Caltun, V. Gafton, L. Leontie, Mater. Res. Bull. **46**, 1455 (2011)
34. W.B. Carpenter, J. A. Fournier, R. Biswas, G. A. Voth, and A. Tokmakoff , The Journal of Chemical Physics **147**, 084503 (2017).
35. S.K. Banerjee, W. O'Reilly, IEEE Trans. Magnets. **3**, 463 (1966)
36. W. Zheng, F. Gao, H. Gu, J. Magn. Mater. **288**, 403 (2005)
37. W.S. Mohamed, M. Alzaid, M.S.M. Abdelbaky, Z. Amghouz, Nanomaterials **9**, 1602 (2019)
38. J.K. Oh, J.M. Park, Prog. Polym. Sci. **36**, 168 (2011)
39. R. Vekariya, K. Patel, H. Patel, Indian J. Chem. **57B**, 576 (2018)
40. J. Zheng, Li. Yiqun. Mendeleev Commun. **280**, 21 (2011)
41. S. Tekale, S. Kauthale, K. Jadhav, R. Pawar, J. Chem. (2013).
42. H. Mecadon, M. Rohman, M. Rajbangshi, B. Myrboh, Tetrahedron Lett. **52**, 2523 (2011)
43. A. Atar, J. Kim, K. Lim, Y. Jeong, Synth. Commun. **44**, 2679 (2014)
44. M. Nasseri, S. Sadeghzadeh, Monatsh Chem. **144**, 1551 (2013)
45. M. Bakherad, A. Keivanloo, M. Gholizadeh, R. Doosti, M. Javanmardi, Res Chem Intermed **43**, 1013 (2017)
46. R. Guo, Z. An, L. Mo, S. Yang, H. Liu, S. Wang, Z. Zhang, Tetrahedron **9331**, 69 (2013)
47. Q. Zhange, B. Liu, W. Chen, Q. Lin, X. Lin, Green Chem. **10**, 972 (2008)
48. K. Pradhan, S. Paul, A.R. Das, Catal. Sci. Technol. **4**, 822 (2014)
49. F. Moeinpour, A. Khojastehnezhad, Chinese Chem. Lett. **26**(5), 575 (2015)
50. F. Moeinpour, A. Khojastehnezhad, Arab. J. Chem. **10**, 3468 (2017)
51. H. Mecadon, R. Md Rumum, M. Rajbangshi, B. Myrboh, Tetrahedron Lett. **52**, 2523 (2011)
52. A. Siddekha, A. Nizam, M.A. Pasha, Spectrochim. Acta A. **81**, 431 (2011)
53. J.B. Gujar, M.A. Chaudhari, D.S. Kawade, M.S. Shingare, Tetrahedron Lett. **55**, 6030 (2014)
54. Y.A. Tayade, S.A. Padvi, Y.B. Wagh, D.S. Dalal, Tetrahedron Lett. **56**(19), 2441 (2015)
55. M. Bihani, P.P. Bora, G. Bez, H. Askari, A.C.S. Sustain. Chem. Eng. **1**, 440 (2013)
56. H. Mecadon, H.; R. Rohman, Md.; I. Kharbangar, B. Laloo, I. Kharkongor, M. Rajbangshi B. Myrboh, Tetrahedron Lett. **52**, 3228 (2011)
57. K.S. Dalal, Y.A. Tayade, Y.B. Wagh, D.R. Trivedi, D.S. Dalal, B.L. Chaudhari, RSC Adv **6**, 14868 (2016)
58. P.P. Bora, M. Bihani, G. Bez, J. Mol Catal. B Enzym. **92**, 24 (2013)
59. M. R. Bhosle, L.D. Khillare, S.T. Dhumal, R.A. Mane Chinese Chem. Lett. 27, 370 (2016)